New insights into the relationship between suture closure and craniofacial dysmorphology in sagittal nonsyndromic craniosynostosis

Yann Heuzé, Simeon Boyadjiev, Jeffrey Marsh, Alex Kane, Elijah Cherkez, James Boggan, Joan Richtsmeier

New insights into the relationship between suture closure and craniofacial dysmorphology in sagittal nonsyndromic craniosynostosis.

Yann Heuzé[1], Simeon A. Boyadjiev[2], Jeffrey L. Marsh[3], Alex A. Kane[4], Elijah Cherkez[2], James E. Boggan[5] and Joan T. Richtsmeier[1]

[1]Department of Anthropology, The Pennsylvania State University, PA, USA.
[2]Section of Genetics, Department of Pediatrics, University of California Davis, Sacramento CA, USA.
[3]St. John's Mercy Children's Hospital, St Louis MO, USA
[4]Washington University School of Medicine, Saint Louis MO, USA
[5]Department of Neurological Surgery, University of California Davis, Sacramento CA, USA

Correspondence
Yann Heuzé, Department of Anthropology, The Pennsylvania State University, 311 Carpenter Building, University Park, PA 16802, USA. T: +1 814 865 2066, F: +1 814 863 1474, E: yuh15@psu.edu
Joan T. Richtsmeier, Department of Anthropology, The Pennsylvania State University, 311 Carpenter Building, University Park, PA 16802, USA. T: +1 814 863 0562, F: +1 814 863 1474, E: jta10@psu.edu

Abstract

Premature closure of the sagittal suture occurs as an isolated (nonsyndromic) birth defect, or as a syndromic anomaly in combination with other congenital dysmorphologies. The genetic causes of sagittal nonsyndromic craniosynostosis (NSC) remain unknown. Though variation of the dysmorphic (scaphocephaly) skull shape of sagittal NSC cases has been acknowledged, this variation has not been quantitatively studied in 3D. We have analyzed the computed tomography skull images of 43 infants (aged from 0.9 to 9 months) with sagittal NSC using anatomical landmarks and semilandmarks to quantify and characterize the within-sample phenotypic variation. Suture closure patterns were defined by dividing the sagittal suture into three sections (anterior, central, posterior) and coding each section as "closed" or "fused". Principal components analysis of the Procrustes shape coordinates representing skull shape of 43 cases of NSC did not separate individuals by sex, chronological age, or dental stages of deciduous maxillary first molar. However, analysis of suture closure pattern allowed separation of these data. The central section of the sagittal suture appears to be the first to fuse. Then, at least two different developmental paths towards complete fusion of the sagittal suture exist; either the anterior section or the posterior section is the second to fuse. Results indicate that according to the sequence of sagittal suture closure patterns, different

craniofacial complex shapes are observed. The relationship between craniofacial shape and suture closure indicates not only which suture fused prematurely (in our case the sagittal suture), but also the pattern in which the suture closes. Whether these patterns indicate differences in aetiology cannot be determined with our data and requires analysis of longitudinal data, most appropriately of animal models where prenatal conditions can be monitored.

Keywords

Isolated craniosynostosis; geometric morphometrics; suture closure pattern; suture closure sequence; dysplastic and compensatory growth; scaphocephaly; skull shape

Introduction

Craniosynostosis is defined as the premature fusion of one or more cranial suture and is a common malformation occurring in 3-5 per 10,000 live births in all ethnic groups (Cohen, 2000). Craniosynostosis of the sagittal suture is the most common form of craniosynostosis accounting for 55-60% of all craniosynostoses (Anderson & Geiger, 1965; Shilito & Matson, 1968; Hunter & Rudd, 1976; Lajeunie et al. 1996). Nonsyndromic (isolated) craniosynostosis (NSC) of the sagittal suture represents the majority of all cases of sagittal synostosis with a birth prevalence of 1.4-1.5 per 10,000 live births (Lajeunie et al. 1996; Boulet et al. 2008). Though environmental and genetic risk factors for craniosynostosis have been identified, no single risk factor has emerged as being necessary or sufficient to cause premature fusion of any of the calvarial sutures. *In utero* head constraint has historically been considered as an environmental component of craniosynostosis (Koskinen-Moffett et al. 1982; Graham, 1998; Cohen, 2000). Twin studies reported by Lajeunie et al. (2005) suggested a multifactorial pattern of inheritance, supporting both an environmental (*in utero* head constraint due to multiple births) and genetic origin in midline craniosynostosis (i.e. metopic and sagittal). Recently, an in vitro model of force-induced sagittal craniosynostosis has corroborated the importance of intrauterine constraint in initiation of midline craniosynostosis (Oppenheimer et al. 2009). Advanced maternal age (35 years and older) and birth weight (>4,000 g) are additional environmental components of sagittal NSC (Boulet et al. 2008).

Little is known about the genetic basis of NSC. FGFR 1, 2, 3 and TWIST are among the genes commonly identified for their involvement in craniosynostosis syndromes (Apert, Crouzon, Pfeiffer, and Saethre-Chotzen syndromes) (Muenke et al. 1994; Hollway et al. 1997), but a role for these genes in NSC has not yet been identified (Sakai et al. 2001; Boyadjiev et al. 2002; Zeiger et al. 2002; Morriss-Kay & Wilkie, 2005; Boyadjiev, 2007).

Sagittal NSC is thought to represent a consistent phenotypic group of unknown aetiology (see for example the 2D quantitative study of Guimarães-Ferreira et al. 2006) that shares a common skull phenotype described as scaphocephalic even if variation in calvarial shape has been reported (Schmelzer et al. 2007). Though current research efforts are focused on identifying subtle associated

phenotypes in other developmental systems (Boyadjiev, 2007), NSC is still thought of as primarily a craniofacial disease.

Since the advent of CT imaging, detailed analysis of the three-dimensional morphology of both the ecto- and endocranial surfaces of the skull has been possible and much has been learned about the facial and cranial base correlates of premature neurocranial suture closure. However, most quantitative analyses have been limited to traditional anthropometric measures or linear measures between anatomical landmarks. Anatomical landmarks are precise locations on biological forms that hold some biological meaning or significance and ensure correspondence among the forms being compared (Richtsmeier et al. 1995). Landmark locations are recorded in 2- or 3D space with an estimated degree of precision and accuracy. Because the cranial vault is relatively devoid of anatomical landmarks, especially in comparison to the density of landmarks on the cranial base and the facial skeleton (Valeri et al. 1998), information pertaining to shape change of the cranial vault is limited when only anatomical landmarks are used. Here, we introduce semilandmarks to the investigation of craniofacial shape of infants with sagittal craniosynostosis. Semilandmarks were introduced to adapt landmark-based statistics to smooth curves in 2D (Bookstein, 1991; 1997), and the algebra was extended to accommodate the analysis of 3D data (Gunz, 2005; Gunz, et al. 2005). Semilandmarks present “deficient” coordinates and require specific computational steps to define their final location on their defined curves or surfaces. After this computational stage, semilandmarks acquire a geometric correspondence across individuals so that comparative analyses can be conducted. The use of semilandmarks allows a more complete characterization of the overall morphology of the cranial vault, a region of high interest in the study of NSC.

Here we investigate skull shape in a sample of infants with sagittal NSC using anatomical landmarks and semilandmarks and appropriate methods of analysis to identify and quantify phenotypic variation in sagittal NSC. Using these data we sequentially test three different hypotheses.

Research Design

Since Virchow’s (1851) study, an implicit assumption of a direct causal relationship between suture closure and cranial vault shape has underlain most craniosynostosis research and treatment protocols. Here we use cross sectional data of a sample of

individuals with sagittal NSC who had not yet undergone any surgery or manipulation to test hypotheses about the relationship between suture closure and cranial shape.

A generally accepted idea is that the earlier the synostosis takes place, the greater the effect on skull shape and, conversely, the later that synostosis occurs, the less effect on skull shape (Cohen, 1986). In the present study, no control sample is considered since our aim is to better characterize sagittal NSC and not to compare its phenotype with the unaffected skull phenotype. Because we did not know the timing of onset of craniosynostosis for individuals in our sample and we did not use a control sample, the relationship between timing of craniosynostosis and effect on skull shape, as well as the notion of severity, could not be tested in the present manuscript. However, the relationship between shape variation and age and sex represent key issues that warrant study. Consequently we test the hypothesis that cranial shape is associated with sex, age, or level of maturity (H1). Support for H1 will be characterized by the identification of different groups of individuals that share common shape features according to their sex, age or level of maturity.

Albright & Byrd (1981) studied the timing of sagittal suture closure in 14 NSC patients. Their results revealed a heterogeneous sequence of closure patterns suggesting variability in fusion of the sagittal suture in sagittal NSC cases. In the present study, we focus on the pattern of closure of the sagittal suture of 43 patients with sagittal NSC. We divide the sagittal suture into three anatomic sections (anterior, central, posterior) and each of these sections is coded to characterize the nature of suture closure (i.e. closed, fused). In the present study a stepwise and irreversible progression is assumed between the different stages of fusion: initially, the suture is patent, then it is closing, and finally it becomes fused. When the sagittal suture is “fused”, no evidence of a suture between the two parietal bones is visible on 3D CT reconstructions. When the sagittal suture (or part of it) is “closed” but not yet fused, the suture remain visible as a fine line. Note that a single sagittal suture can present a closure pattern involving different stages (e.g. a sagittal suture fused in its central and anterior sections but closed in its posterior section). We refer to the resulting set of observations as the “closure pattern”. During craniofacial development, the sagittal suture will present different closure patterns. It is then possible to study the sequence of these closure patterns. Sequence as used in this paper is different from timing and does not imply any reference to absolute time. The timing of a specific event (e.g. sagittal suture fusion) includes the moment when this event starts and ends,

and its duration. Even if results of cross sectional studies based on large sample can be extrapolated to describe the timing of an event, only longitudinal studies provide the information required to define the timing of an event. In the present cross-sectional study we only describe different sequences of suture closure patterns and do not focus on timing. From our data on closure pattern, we test a second hypothesis that a unique sequence of sagittal suture closure patterns is associated with sagittal NSC (H2).

Virchow (1851) proposed that cranial deformity found in subjects with craniosynostosis could be explained by growth inhibition at right angles to the fused suture, with compensatory overexpansion of the cranium at patent sutural sites accommodating normal growth of the brain. Since then, this concept of dysplastic and compensatory growth has been shown to involve not only the calvaria, but all regions of the craniofacial complex in patients with different types of craniosynostosis (Kreiborg, 1986). Though a heterogeneous aetiology has been suggested, (Boyadjiev, 2007) samples of sagittal NSC individuals have implicitly been considered as representing a single, albeit variable, calvarial phenotype (scaphocephaly). Some have tried to quantitatively address the phenotypic variation of NSC (Richtsmeier et al. 1995) with limited success. Difficulties stem from the relatively small sample sizes, the varied quality of image data, and the specific quantitative approaches used in analysis. Here we take full advantage of available data and recently developed tools to quantify shape variation and investigate in 3D detail the potential relationship between the closure patterns sequence of the sagittal suture and corresponding skull shape. We test a third hypothesis that different sagittal suture closure pattern sequences generate different craniofacial shapes (H3).

Materials and methods

Images

Computed tomography (CT) images of children diagnosed with sagittal NSC were acquired from several medical centers (John Hopkins Hospital; Children's Hospital – Boston; University of Oklahoma Medical Center; Washington University), some of which participate in the International Craniosynostosis Consortium

(genetics.ucdmc.ucdavis.edu). These images were deposited into the Image Analysis and Morphometrics Laboratory archive housed at the Pennsylvania State University (getahead.psu.edu). Here we analyze data from the images of 43 individuals diagnosed with sagittal NSC. Individuals diagnosed with a known genetic syndrome were excluded and none of the individuals included in our study sample had extracranial anomalies. For 22 out of 43 individuals, a detailed clinical genetics evaluation was done by hot-spot mutation analysis of the areas associated with known craniosynostosis syndromes (FGFR1 exon IIIa, FGFR2 exons IIIa and IIIc, FGFR3 exon IIIa, and the entire coding sequence of TWIST). None of these 22 individuals carried any of the known mutations. Our sample consequently consists of 22 individuals who did not express any of these known mutations and 21 individuals with a clinical diagnosis of sagittal NSC for who molecular data was not available. At the time of CT exam, infants had not undergone any surgical procedure and ranged in age from 0.9 to 9.0 months (mean age: 4.7 months, sd: 2.2 months) (Table 1). Infants were classified into three-month age intervals for subsequent analyses. The sample includes a majority of males (i.e. 35 males, 8 females), which reflects the male to female ratio reported for sagittal synostosis (e.g., 7:3 to 4:1: Shilito & Matson, 1968; Hunter & Rudd, 1976; Lajeunie et al. 1996).

Closure of the sagittal suture

Because individuals within this sample were medically diagnosed with sagittal NSC (criteria for inclusion in the present study), all have premature fusion of the sagittal suture. However, we found that the exact condition of the sagittal suture is not identical for all individuals. We scored the condition of the sagittal suture as either totally or partially fused (Fig. 1). When the sagittal suture is ‘fused’, no evidence of a suture between the two parietal bones is visible on 3D CT reconstructions. When the sagittal suture (or part of it) is ‘closed’ but not yet fused, the suture remains visible as a fine line. Note that “closed” as used in the present study is sufficient to diagnose sagittal craniosynostosis.

In the present study, we divided the sagittal suture into three sections based on anatomical location: anterior, central, posterior, and each section was scored as fused (F) or closed (C). Infants with a completely fused sagittal suture were coded as “FFF” (i.e. the anterior, central, and posterior sections of the sagittal suture are fused). Infants whose sagittal suture was fused anteriorly but closed posteriorly were

coded as “FFC” or “FCC” according to the status of the central section of the suture. Finally, infants whose sagittal suture was closed anteriorly and fused posteriorly were coded as “CFF” or “CCF” according to the status of the central section of the suture (Table 1).

Dental development stage assessment

Chronological age of each individual at CT exam was computed by determining the number of days between the date of birth and the date of the CT exam. However, since all of our subjects are infants, it is possible that chronological age may be biased because our sample might include infants born prematurely or who experience some sort of developmental or growth delay. Unfortunately we do not have access to data regarding gestational age for all the individuals in our sample. To address this potential bias and to determine a degree of maturity for each individual in our sample, dental development stage of each infant was assessed using the deciduous maxillary first molar (m^1). We adopted the radiographic method originally proposed by Demirjian et al. (1973) for permanent teeth and transposed to deciduous teeth by Liversidge & Molleson (2004) as adapted to 3D CT reconstructed deciduous teeth by Bayle et al. (2009). Although eight stages are defined from the first signs of mineralisation of the cuspids (stage A) to the completion of the root(s) (stage H1), the relatively young age range of our sample limits us to the crown formation stages (A to D) (Fig. 2). We used thresholding tools to segment tooth anatomy and therefore most likely underestimated the degree of dental mineralisation. However since we used the same tool for every individual, this potential underestimation is consistent across individuals in our sample. In the present study, no attempt was made to link the degree of maturity assessed by means of dental stages to chronological age. Consequently, we do not refer to any biological or developmental age, but only to a certain degree of maturity.

Landmark data collection

Images were reconstructed using a threshold that enabled visualization of bone. A set of 33 anatomical landmarks (LM) were defined and located on the 3D reconstruction of the CT images of each infant and the corresponding x,y,z coordinates were recorded (Table 2, Fig. 3). The 3D reconstructions of the CT images were manually closed using a segmentation tool at the region of the patent

fontanelles to allow the placement of landmarks in these regions. In addition to the anatomical landmarks, a total of 189 semilandmarks were defined on four predefined curves (53 curve semilandmarks; CL) and four surface patches (136 surface semilandmarks; SL) on each skull. In order to gain geometric correspondence, semilandmarks were “slid” or moved along these curves and patches according to a sliding algorithm that minimizes the bending energy (Bookstein, 1997; for a more detailed description of the definition, recording and treatment of the semilandmarks see supplementary data 1).

Superimposition and exploration of the shape space

The 43 individuals defined on the basis of 222 landmarks (anatomical and semilandmarks combined) were superimposed by translating, rotating and scaling all forms with the aim of reducing the sum of the squared distances between homologous landmarks by means of a general Procrustes analysis (Rohlf & Slice, 1990). The coordinates of the resulting centered, scaled, and rotated landmarks are called the Procrustes shape coordinates. A measure of overall size called centroid size (CS; the square root of the sum of the squared distances of the landmarks to the centroid) was estimated for each individual and used as a proxy for overall cranial size in subsequent analyses. Centroid size is a measure of scale for landmark configurations, which has been shown to be approximatively uncorrelated with shape for small isotropic variation (Bookstein, 1991; Dryden & Mardia, 1998). A Procrustes average shape (PAS) is computed as the coordinate-wise average of the Procrustes shape coordinates.

The Procrustes shape coordinates were analyzed by a principal components analysis to reduce the dimensionality of the dataset and explore the placement of individuals within the shape space. The eventual goal is to study the specific combination of morphological variables that successfully separate individuals into groups of known membership by projecting them onto the shape space. PCA is computed by an eigendecomposition of the sample covariance matrix and is a rigid rotation of the data preserving the Procrustes distances among individuals. The eigenvectors (or principal components, PCs) contain the weightings for the linear combination of the original variables and can be visualized as actual shape deformation (Mitteroecker & Gunz, 2009). A simulation of a continuous shape deformation based on the available data can be obtained by warping the PAS to the

negative (or positive) direction of the principal component. This is done simply by adding a multiple of the eigenvector to the mean shape (PAS). A warping through the negative direction will produce a deformation that is the inverse of a warping through the positive direction. The warping was executed by thin-plate spline (TPS; Bookstein, 1991).

Software

Amira 4.0.1 (Mercury Computer Systems Inc.) was used to visualize the CT images, to segment and reconstruct the skulls, to measure anatomical landmarks, and to do surface warping using TPS (Bookstein, 1991). The surface semilandmarks were measured on the template in Landmarks v3.0.0.6 (Wiley et al. 2005).The semiautomatic procedure allowing the measurement of the semilandmarks on the target skulls using TPS was done in Viewbox 4.0.0.98 (dHAL software, Athens, Greece). The Procrustes superimposition and subsequent statistical analysis were done using MorphoJ 1.01a (Klingenberg, 2008).

Results

The PCA of the Procrustes shape coordinates using all landmarks and semilandmarks of the 43 infants with sagittal NSC was computed. No separation of the data according to sex or age (grouped by 3-month intervals) was observed with the first 10 PCs accounting for a total of 82% of the total variance (see Fig. 4 for a plot of PC1 and PC2). A lack of separation among groups for the first 10 PCs persisted when the dental stage of the deciduous first molar (m^1, Table 1) was substituted for the 3-month age groups in the PCA (not shown). No separation of individuals according to the availability of molecular data was observed with the first 10 PCs (not shown). Multivariate regression between CS (size; independent variable) and the first 10 PCs (shape; dependent variables) indicated that size only accounts for 4.5% of shape variation (percentage predicted = 1 - [sums of squares error/sums of squares total]). A permutation test (10,000 rounds) against the null hypothesis of independence between size (CS) and shape (first 10 PCs) gives a P-value of 0.053. Similar results were obtained when size was replaced by age (percentage predicted:

4.5; permutation test P-value: 0.058). A PCA of the residuals of the regression of the PCs coefficient with CS resulted in almost identical placement of the individuals as the one obtained with the PCA of the Procrustes coordinates.

In only two individuals out of 43 was the central section of the sagittal suture closed but not yet fused. The youngest child of the sample shows the pattern FCC and another individual shows the pattern CCC. Of the 41 remaining individuals, each child exhibited complete fusion (F) of the central region of the sagittal suture. However, we found the following variation in other sections of the suture: 10 individuals showed the anterior and posterior sections closed (i.e. CFC); seven displayed the anterior section closed and the posterior section fused (i.e. CFF); and eight individuals exhibited the anterior section fused and the posterior section closed (i.e. FFC). Finally, the sagittal suture was totally fused (i.e. FFF) in 16 individuals.

Considering the relationship between overall size (CS being highly correlated with age; R^2=0.7628, $p<0.001$) and closure patterns, individuals showing the CFC closure patterns were significantly smaller (mean CS: 91.1) than: (1) individuals showing the pattern CFF (mean CS: 96.2) (t test, p= 0.036); (2) individuals showing the pattern FFC (mean CS: 96.3) (t test, p=0.019); and (3) individuals showing the pattern FFF (mean CS: 98.7) (t test, p=0.001). Individuals showing the CFF and FFC closure patterns were of equal mean sizes (Fig. 5).

In contrast to sex, chronological age and m^1 dental stages, the sagittal suture closure patterns allowed a separation of the 43 individuals according to skull shape as estimated by the PCA of the Procrustes shape coordinates (Fig. 6). Indeed, the individuals coded as FFC showed negative PC1 scores, while the individuals coded as CFC and CFF showed positive PC1 scores. Though the demarcation was not as clear as with PC1, individuals coded as CFC (negative scores) are separated from those coded as CFF (positive scores) along PC2.

Exploration of the shape continuum associated with the negative and positive PC scores allows the observer to better understand the information expressed by the PCA. The main differences between a warped skull corresponding to -0.05PC1 and a warped skull corresponding to +0.04PC1 were mainly located on the cranial vault and the cranial base. Few differences were noted for the face (Fig. 7). The anterior frontal of a warped skull corresponding to +0.04PC1 is supero-inferiorly elongated and

protrudes anteriorly above glabella (Fig. 7, arrows A, E). The bregma is relatively “higher”. The occipital is convex and more inferoposteriorly projected with a “lower” lambda (Fig. 7, arrow C). In lateral profile, the posterior sections of the parietals are more inferiorly positioned and formed a more concave profile (Fig. 7, arrow B). In a supero-inferior view, the skull appears more elongated in the anteroposterior direction and the medial and posterior crania fossae are narrower (Fig. 7, arrows F, G). The cranial base, especially the middle and posterior fossae, is more posteriorly shifted, as seen with the petrous temporal bones and the occipital (Fig. 7, arrows C, D, F).

Regarding PC2, the main differences between a warped skull corresponding to -0.04PC2 and a warped skull corresponding to +0.04PC2 were located on the face, the cranial base, and the posterior section of the cranial vault (parietal and occipital bones) (Fig. 7). A warped skull corresponding to +0.04PC2 demonstrates a wider upper face, wider orbits associated with a broader interorbital distance, and a relatively less anteriorly projected face. The cranial base, especially the anterior and middle cranial fossae, is more inferiorly projected, or depressed (Fig. 7, arrow J). The anterior and middle crania fossae are wider while the posterior crania fossa is narrower (Fig. 7, arrow K). The posterior section of the parietals and the occipital are less posteriorly projected but present a similar profile to that of a warped skull corresponding to -0.04PC2 (Fig. 7, arrows H, I, L).

Discussion

Deformation of the cranial vault has been observed as a defining characteristic in craniosynostosis since its definition. Qualitative assessment of calvarial dysmorphology has shown consistent variability in sagittal NSC (Schmelzer et al. 2007). Quantitative analysis of the cranial vault has proven problematic due to its smooth contours and relative lack of characteristic locations that can be used to precisely place anatomical landmarks. Using geometric morphometric methods developed for the placement and analysis of semilandmarks, we have provided 3D information on cranial shape variation in sagittal craniosynostosis including detailed information about vault shape. As a consequence, we are able to study the

relationship of premature fusion of the sagittal suture with the overall shape of the cranium.

H1: Cranial shape in sagittal NSC is associated with sex, age, or level of maturity

When sex, chronological age, and level of maturity assessed by means of m^1 were used as classifiers with the PCA of the Procrustes shape coordinates, no obvious separation of the data was seen. Multivariate regression between age and shape (first 10 PCs) indicated that age only accounts for 4.5% of shape variation. Hypothesis 1 is not supported by these results which imply that shape variation as registered by the first 10 PCs was not associated with sex, age or level of maturity. In addition, multivariate regression between size and shape (10 first PCs) showed that size only accounts for 4.5% of shape variation, while a PCA of the residuals of the regression of shape with size produced almost identical placement of the individuals to the one obtained in the shape space. Consequently, allometry was not the main source of shape variation. Although we cannot address the “severity” of shape dysmorphology in this sample of sagittal NSC due to the lack of a control sample, our analysis demonstrates that neither chronological age nor level of maturity explain the shape variation quantified for this sample of 43 children with sagittal NSC. Our results may reflect the limited age range of this sample (i.e. 0.9 to 9 months). Because the great majority of reconstructive surgeries are done before the age of one year, we were not able to study the influence of sagittal NSC on the shape of the craniofacial complex after the first year of life.

H2: A unique sequence of sagittal suture closure patterns is associated with sagittal NSC

By coding closure pattern of the sagittal suture we gain access to the sequence leading from a patent sagittal suture to a fused one. Our analysis depends on the principle that a stepwise and irreversible progression exists between the different stages of fusion defined in the present study: initially, the suture is open, then it is closing (C), and finally it becomes fused (F). Careful observations show that different stages of fusion can be found simultaneously across the sagittal suture. For this reason we divided the sagittal suture into three distinct sections and qualitatively assessed and scored each section. Since the central section of the sagittal suture is

the region that was most often fused (95.6%, Table 1), we suggest that it is frequently the section of the suture that closes first. This confirms previous observations made by Vannier (2000). The co-occurrence of the sagittal suture closure patterns CFF and FFC in roughly equal numbers (Table 1) does not support the hypothesis of a unique sequence of closure patterns since by definition closure (C) cannot follow fusion (F). The equal mean sizes of CFF and FFC (Fig. 5) also indicate the coexistence of multiple sequences of closure patterns. At least two different paths towards complete fusion (FFF) appear to exist in the sample. Either the anterior section will be the second part of the sagittal suture to fuse (FFC), or the posterior section will be the second part to fuse (CFF). A third sequence of closure patterns could exist if the anterior and posterior sections of the sagittal suture fused roughly in the same time (Fig. 8). The coexistence of at least two different sequences of closure patterns for the fusion of the sagittal suture in sagittal NSC does not support the hypothesis of a unique sequence of closure patterns (H2) and confirms results of a previous analysis of a small sample which showed various closure patterns of the sagittal suture (Albright & Byrd, 1981).

H3: Different pattern sequences of sagittal suture closure generate different craniofacial shapes

Of the variables considered (sex, chronological age, dental stages of m^1 and sagittal suture closure pattern), suture closure pattern is the only variable associated with placement of individuals on the plot of the PCA of the Procrustes shape coordinates of the 43 individuals (Fig. 6). Skull shapes that characterize the negative end of PC1 were associated with an expanded temporal width, a relatively “low” bregma, and a relatively flat occipital with a “high” lambda. In addition to the individuals showing the pattern FFF who were homogeneously distributed, the individuals plotted on the negative end of PC1 share the sagittal suture closure pattern FFC. Following the concept of dysplastic and compensatory growth of the craniofacial complex, we interpret the expanded temporal width, the superoposteriorly expanded parietals and the relatively “low” bregma and “high” lambda as corresponding with premature fusion of the median and anterior sections of the sagittal suture. In this interpretation, the posterior section of the sagittal suture is the last section to close, remaining patent and thereby experiencing the maximum of local compensatory growth. Individuals with positive PC1 scores are associated with a skull shape characterized

by relatively superiorly placed bregma and a relatively inferiorly placed lambda, a relatively more convex and more inferoposteriorly projected occipital, a narrower posterior half of the skull, and a posteriorly and inferiorly displaced cranial base (Fig. 7). In addition to those individuals showing the pattern FFF who were homogeneously distributed, individuals situated on the right side of the PCA plot (i.e. those with positive PC1 scores) shared the patterns CFC and CFF. Finally, the posterior section of the metopic suture was largely patent in the majority of individuals (15 individuals out of 17) showing the closure patterns CFC and CFF (positive PC1 scores). In these cases, the anterior fontanelle took on a triangular or a more rectangular shape (as seen in Fig. 3). The individuals showing the closure patterns FFC (negative PC1 scores) presented a posterior section of the metopic suture that was largely patent in only 2 out of 7 cases. At least two different interpretations can be made about the presence of this large patent area: (1) the patent area is likely associated with the localized overgrowth of the frontal region; or (2) the patent area potentially reflects the compensation for increased intracranial pressure due to the constraint on calvarial width expansion.

Consideration of PC2 reveals a separation among the suture closure patterns CFC and CFF. Individuals with positive PC2 scores correspond to the pattern CFF and the corresponding warped skull (+0.04PC2) presented a relatively wider face and frontal portion of the skull (but a narrower occiput), a relatively reduced anteroposterior dimension, and a cranial base that is relatively more inferiorly placed (Fig. 7). Following the concept of dysplastic and compensatory growth of the craniofacial complex, we suggest that the individuals at the positive end of PC2 reveal a craniofacial shape that is a consequence of the premature fusion of the middle and posterior sections of the sagittal suture, which generates a physical constraint driving a compensatory response mainly located in the anterior part of the skull and along the supero-inferior axis.

Instead of using skulls warped according to the negative or positive direction of the eigenvector, it is also possible to compute and then compare Procrustes average shapes (PAS) according to the sagittal suture closure pattern. The PAS of all individuals showing the closure pattern CFC was computed, as were the PAS of all the individuals showing the closure pattern CFF, and the PAS of all individuals showing the closure pattern FFC. Because the PCA of the Procrustes shape coordinates of the 43 individuals allows for good separation between individuals

according to their closure pattern, this alternative approach allows similar observations than those made with the warped skulls. Supplementary data 2 and 3 present this alternative approach based on the PASs.

Since Virchow (1851), several studies on craniosynostosis have produced results supporting the concept of dysplastic and compensatory growth of the craniofacial complex (e.g. Kreiborg, 1986). Virchow (1851) thought the primary cause was the premature fusion of a cranial suture and that cranial base deformation followed. Moss (1954, 1975) proposed the functional matrix hypothesis which introduced the role of soft tissues in cranial growth. He argued that cranial base dysmorphology result in aberrant tensile forces being communicated from the brain to the calvarium via dural attachments, ultimately causing craniosynostosis. Although our study does not support either of these theories in particular, it shows a strong relationship between the sequence of the closure pattern of the sagittal suture and deformation of the cranium. Our results add to the well recognized relationship between craniofacial shape and premature suture closure. For premature closure of the sagittal suture, our results suggest that the shape of the craniofacial complex not only identifies the sagittal suture as the suture that is closed prematurely but also the pattern in which the suture closes.

By analyzing variation in skull shape in a cross sectional sample of children with sagittal NSC we participate in a more general effort aimed at the understanding of the aetiology of this disorder and thereby adding to the formulation of clinical rules for craniofacial surgery and neurosurgical treatment that contribute to skull shape (e.g. Delashaw et al. 1989; Marsh, 2000). Multiple surgical techniques are available for the treatment of sagittal NSC. It is most important, that the surgical approach be suited to the age of the patient, the state of suture fusion and the particular deformity. Besides the general scaphocephaly, anterior or posterior bulging of the skull and temporal indentation can be major problems that require appropriate variation in technique (Jane & Persing, 2000). Importantly, none of the 43 individuals (including our youngest individual aged about one month) showed a section of the sagittal suture still patent. Consequently, the closure of at least the central section of the sagittal suture most likely takes place prenatally, suggesting that sagittal NSC is a congenital malformation. We suggest that prenatal ultrasound could be used for third

trimester prenatal diagnosis which could aid the family and the medical team for optimal monitoring of the patient.

Our results suggest a relationship between pattern and sequence of suture closure in sagittal NSC and calvarial dysmorphology. Tests of our results require different and possibly large samples where factors known to potentially influence skull shape are known (e.g. ethnicity, duration and condition of labour). Whether the patterns we have quantified indicate differences in aetiology cannot be determined with our data, but require longitudinal studies, most appropriately of animal models where prenatal conditions can be manipulated and monitored.

Acknowledgments

We are grateful to all study participants and to the following persons who participated in the data collection and management: Daniel Govier from Washington University; Jayesh Panchal from Oklahoma City Children's Hospital; Craig Senders, Travis Tollefson and Bridget Wilson from University of California Davis; Virginia Kimonis from University of California Irvine; Nisha Isaac, Doris Lin, George Jallo, Ben Carson, and Craig Vander Kolk from the Johns Hopkins Medical Institutions; Caroline D. Robson and Joan Stoler from the Children's Hospital Boston; Satama Sirivunnabood from Pennsylvania State University. We thank Neus Martínez-Abadías for early fruitful discussion of this manuscript. We thank Brenda C. Frazier, Chris Percival and John M. Starbuck for editorial suggestions. We thank the two anonymous referees for their constructive comments that helped to enhance the overall quality of this manuscript.

This study was funded by Public Health Service grants R01 DE018500, 3R01DE18500-02S1, R01 DE016886, and CDC 5R01DD000350. SAB is partially supported by Children's Miracle Network (CMN) endowed chair in Pediatric Genetics.

References

Albright AL, Byrd RP (1981) Suture pathology in craniosynostosis. *J Neurosurg* **54**, 384-387.

Anderson FM, Geiger LE (1965) Craniosynostosis: a survey of 204 cases. *J Neurosurg* **22**, 229-240.

Bayle P, Braga J, Mazurier A, Macchiarelli R (2009) Dental developmental pattern of the Neanderthal child from Roc de Marsal: a high-resolution 3D analysis. *J Hum Evol* **56**, 66-75.

Bookstein FL (1991) *Morphometric tools for landmark data: geometry and biology*. Cambridge: Cambridge University Press.

Bookstein FL (1997) Landmark methods for forms without landmarks: Morphometrics of group differences in outline shape. *Med Im Anal* **1**, 225-243.

Boulet SL, Rasmussen SA, Honein MA (2008) A population-based study of craniosynostosis in Metropolitan Atlanta, 1989-2003. *Am J Med Gen Part A* **146A**, 984-991.

Boyadjiev SA (2007) Genetic analysis of non-syndromic craniosynostosis. *Orthod Craniofacial Res* **10**, 129-137.

Boyadjiev SA, Zhang G, Ingersoll R, et al. (2002) Analysis of candidate genes for non-syndromic craniosynostosis. *Am J Hum Genet* **71**, A1795.

Cohen MM Jr. (1986) Perspectives on craniosynostosis. In *Craniosynostosis: diagnosis, evaluation, and management* (ed. Cohen MM Jr.), pp. 21-57. New York: Raven Press.

Cohen MM Jr. (2000) Epidemiology of craniosynostosis. In *Craniosynostosis: diagnosis, evaluation, and management. Second edition* (eds. Cohen MM Jr. & MacLean RE), pp. 112-118. New York: Oxford University Press.

Delashaw JB, Persing JA, Broaddus WC, Jane JA (1989) Rules for cranial vault growth. *Neurosurgery* **70**, 159-165.

Demirjian A, Goldstein H, Tanner JM (1973) A new system of dental age assessment. *Hum Biol* **45**, 211-227.

Guimarães -Ferreira J, Gewalli F, David L, et al. (2006) Sagittal synostosis: I. Preoperative morphology of the skull. *Scand J Plast Reconstr Surg Hand Surg* **40**, 193-199.

Graham JM Jr. (1998) Craniofacial deformation. *Balliere's Clin Paediatr* **6**, 293-315.

Gunz P (2005) Statistical and geometric reconstruction of hominid crania: Reconstructing australopithecine ontogeny. Ph.D. thesis, University of Vienna, Vienna.

Gunz P, Mitteroecker P, Bookstein FL (2005) Semilandmarks in Three Dimensions. In *Modern Morphometrics in Physical Anthropology* (ed. Slice DE), pp. 73-98. New York: Kluwer Academic/Plenum Publishers.

Hollway GE, Suthers GK, Haan EA, et al. (1997) Mutation detection in FGFR2 craniosynostosis syndromes. *Hum Genet* **99,** 251-255.

Howells WW (1973) Cranial Variation in Man. A Study by Multivariate Analysis of Patterns of Difference among Recent Human Populations. *Papers of the Peabody Museum of Archaeology and Ethnology* **67**, 1-259.

Hunter AGW, Rudd NL (1976) Craniosynostosis. I. Sagittal synostosis: its genetics and associated clinical findings in 214 patients who lacked involvement of the coronal suture(s). *Teratology* **14**, 185-193.

Jane JA, Persing JA (2000) Neurosurgical treatment of craniosynostosis. In *Craniosynostosis: diagnosis, evaluation, and management. Second edition* (eds. Cohen MM Jr. & MacLean RE), pp. 209-227. New York: Oxford University Press.

Klingenberg CP (2008) MorphoJ. Faculty of Life Sciences, University of Manchester, UK. http://www.flywings.org.uk/MorphoJ_page.htm

Koskinen-Moffett LK, Moffett BC Jr., Graham JM Jr. (1982) Cranial Synostosis and intra-uterine compression: a developmental study of human sutures. *Prog Clin Biol Res* **10**, 365-378.

Kreiborg S (1986) Postnatal growth and development of the craniofacial complex in premature craniosynostosis. In *Craniosynostosis: diagnosis, evaluation, and management* (ed. Cohen MM Jr.), pp. 157-189. New York: Raven Press.

Lajeunie E, Le Merrer M, Bonaïti-Pellie C, Marchac D, Renier D (1996) Genetic study of scaphocephaly. *Am J Med Genet* **62**, 282-285.

Lajeunie E, Darach WC, Arnaud E, Renier D (2005) Genetic considerations in nonsyndromic midline craniosynostoses: a study of twins and their families. *J Neurosurg (Pediatrics 4)* **103**, 353-356.

Liversidge HM, Molleson T (2004) Variation in crown and root formation and eruption of human deciduous teeth. *Am J Phys Anthropol* **123**, 172-180.

Marsh JL (2000) Surgical research on craniosynostosis. In *Craniosynostosis: diagnosis, evaluation, and management. Second edition* (eds. Cohen MM Jr. & MacLean RE), pp. 292-306. New York: Oxford University Press.

Mitteroecker P, Gunz P (2009) Advances in geometric morphometrics. *Evol Biol* **36**, 235-247.

Moss ML (1954) Growth of the calvaria in the rat: The determination of osseous morphology. *Am J Anat* **94**, 333-362.

Moss ML (1975) Functional anatomy of cranial synostosis. *Childs Brain* **1**, 22-33.

Morriss-Kay GM, Wilkie AOM (2005) Growth of the normal skull vault and its alteration in craniosynostosis: insights from human genetics and experimental studies. *J Anat* **207**, 637-653.

Muenke M, Schell U, Hehr A, et al. (1994) A common mutation in the fibroblast growth factor receptor 1 gene in Pfeiffer syndrome. *Nat Genet* **8,** 269-274.

Oppenheimer AJ, Rhee ST, Goldstein SA, Buchman SR (2009) Force-induced craniosynostosis in the murine sagittal suture. *Plast Reconstr Surg* **124**, 1840-1848.

Richtsmeier JT, Paik CH, Elfert PC, Cole TM 3rd, Dahlman HR (1995) Precision, repeatability and validation of the localization of cranial landmarks using computed tomography scans. *Cleft Palate Craniofac J* **32**, 217-227.

Rohlf F, Slice D (1990) Extensions of the Procrustes method for the optimal superimposition of landmarks. *Syst Zool* **39**, 40-59.

Sakai N, Tokunaga K, Yamazaki Y, et al. (2001) Sequence analysis of fibroblast growth factor receptor 2 (FGFR2) in Japanese patients with craniosynostosis. *J Craniofac Surg* **12,** 580-585.

Schmelzer RE, Perlyn CA, Kane AA, Pilgram TK, Govier D, Marsh JL (2007) Identifying reproducible patterns of calvarial dysmorphology in nonsyndromic sagittal craniosynostosis may affect operative intervention and outcomes assessment. *Plast Reconstr Surg* **119**, 1546-1552.

Shilito J Jr., Matson DD (1968) Craniosynostosis. A review of 519 surgical patients. *Pediatrics* **41**, 829-853.

Valeri CJ, Cole TM 3rd, Lele S, Richtsmeier JT (1998) Capturing data from three-dimensional surfaces using fuzzy landmarks. *Am J Phys Anthropol* **107**, 113-124.

Vannier MW (2000) Radiologic evaluation of craniosynostosis. In *Craniosynostosis: diagnosis, evaluation, and management. Second edition* (eds. Cohen MM Jr. & MacLean RE), pp. 147-174. New York: Oxford University Press.

Virchow R (1851) Ueber den cretinismus, namentlich in Franken, und ueber pathologische Schädelformen. *Verh Phys Med Ges Würzburg* **2**, 230-271.

Wiley DF, Amenta N, Alcantara DA, et al. (2005) Evolutionary morphing. *Proceedings of IEEE Visualization 2005*.

Zeiger JS, Beaty TH, Hetmanski JB, et al. (2002) Genetic and environmental risk factors for sagittal craniosynostosis. *J Craniofac Surg* **13**, 602-606.

Supplementary Material

Supplementary data 1:

Semilandmarks definition and recording

To create the model for placement of semilandmarks, one individual of the sample was arbitrarily selected as the template skull. The template skull is the skull on which all the landmarks and semilandmarks were “manually” placed. Consequently, even though the choice of template skull is arbitrary, this choice will have an effect on the placement of landmarks on all other skulls (Fig. 3). The template was subsequently used in a semiautomatic procedure to determine the location of semilandmarks on all the remaining skulls of the sample called the target skulls. For the target skulls, only the 33 anatomical landmarks and the 4 curves were “manually” measured and recorded. The four curves recorded on each skull were:

1. an open curve describing the mid-sagittal plane (from nasale to opisthion passing by bregma and lambda)
2. two closed curves describing the right and left orbits (each starting and ending at the fronto-zygomatic suture and following the orbital ridge)
3. a closed curve describing the nasal aperture (starting and ending at the nasale, passing by the anterior nasal spine and following the nasal aperture ridge)

On the template skull, the 53 curve semilandmarks were distributed at equal intervals along the defined curves. The positions of the semilandmarks of the target skulls were computed by means of thin-plate spline algorithm (TPS, Bookstein, 1991). Seventeen CLs were distributed along the mid-sagittal plane, 14 CLs were distributed around each of the orbit curves, and 8 CLs were distributed around the nasal aperture curve.

The method for determining the location of surface semilandmarks on the template is more complex. First, four surfaces patches were defined: the frontal patch, the left and right parietal-temporal patches, and the occipital patch. These patches were anchored by controlling points which were, when it was possible, actual anatomical landmarks (not necessarily among the 33 included in this study). Once each patch was defined, a grid was created and superimposed on the skull surface. The intersection of perpendicular lines of the grid defines the position of a

semilandmark. By looking at the figure 3, one can easily imagine the grids used in this study. Because different patches share one or several edges, as a final step repetitive semilandmarks were manually deleted.

Although anatomical landmarks correspond across individuals due to commonalities of development and anatomy, this is not the case for semilandmarks. Still, the defined curves and/or surfaces on which the semilandmarks lie correspond across individuals (e.g., the right orbit curve of a skull A corresponds to the right orbit curve of a skull B) making them useful in determining similarities and differences across shapes.

Contrary to classic anatomical landmarks, semilandmarks present “deficient” coordinates. For instance, a curve semilandmark will have well-defined coordinates on two axes but the coordinate on the third axis depends on the defined curve. The specific location of semilandmarks is adjusted by allowing them to “slide” along the defined curve (curve semilandmarks) or surface (surface semilandmarks) until a specified measure of shape difference among the configurations is minimized (Bookstein, 1997; Gunz et al. 2005). In actuality, to linearize the problem, the semilandmarks do not slide on the defined curve or surface, but instead on the tangent vector to the curve or the tangent plane to the surface. Semilandmarks “slide” along the defined curve or surface through an iterative process repeating the following three steps as outlined by Mitteroecker & Gunz (2009): (1) computation of a tentative sample mean shape and of the tangent vectors for each semilandmark in each individual, (2) sliding of semilandmarks along the tangents to minimize “a specified measure of shape difference” to the mean, and (3) placing back the slid semilandmarks to the nearest point on the curve or the surface, as they may slip off the curvature.

The sliding process can be based on one of two minimization criteria: one algorithm is based on minimizing the “bending energy” (Bookstein, 1997), while the other, based on a Procrustes algorithm minimizes Procrustes distances (Bookstein et al. 2002). Application of either of these criteria causes the semilandmarks to slide along the defined curves or surfaces until they are placed in a location consistent with minimization of the chosen criteria. In the presence of limited shape variation the differences between the two minimization criteria have little effect.

The minimization calculation that determines the sliding of the semilandmarks to their final location confers a correspondence among the forms being analyzed that

is both geometric due to the calculations used and biological due to the biological correspondence of the curves and surfaces under consideration. Once this correspondence is established, semilandmarks are analyzed using the same procedures adopted for anatomical landmarks in the subsequent statistical analyses. Methods for determining the position of semilandmarks are designed to operate on smooth curves and surfaces. These methods become inappropriate as soon as the relative smoothness of the structure of interest diminishes.

Once the semilandmarks are located on the template skull, a semiautomatic procedure is utilised to place the semilandmarks on each target skull. This procedure relies on a warping of the template skull onto the target skull using TPS (Bookstein, 1991). As stated earlier, the 3D coordinates of the 33 anatomical landmarks as well as the location of the four curves are recorded by hand. A TPS is then computed between the template and the target using only the anatomical landmarks (Fig. 3 – blue points) to warp the curve (Fig. 3 – red points) and surface semilandmarks (Fig. 3 – green points) from the template to the target. Finally, a new TPS based on all landmarks and semilandmarks is computed. At this point semilandmarks are slid according to the chosen sliding process. Here we used the sliding algorithm that minimizes the bending energy (Bookstein, 1997). This semiautomatic operation is repeated for each target skull of the sample.

References

Bookstein FL, Streissguth AP, Sampson PD, Connor PD, Barr HM (2002) Corpus callosum shape and neuropsychological deficits in adult males with heavy fetal alcohol exposure. *Neuroimage* **15**, 233-251.

Supplementary data 2

Placement of the individuals on PC1 and PC2 in the shape space defined by the principal components analysis of the Procrustes shape coordinates using all landmarks and semilandmarks of the 43 infants with sagittal NSC. Individuals are coded for suture closure pattern. The key is the same as in Fig. 6. Procrustes average shape (PAS) of the skulls with the closure pattern FFC is represented in blue. PAS of the skulls with the closure pattern CFC is represented in green. PAS of the skulls with the closure pattern CFF is represented in orange. Arrows indicate direction of possible compensatory growth related to suture sections which are closed (dashed lines) opposed to suture sections which are fused (full lines). Because PC1 and PC2 allow the separation of the individuals according to their closure pattern (CFC, CFF, and FFC), one can observe similarities between Procrustes average shape skulls represented here and corresponding warped skull represented in Fig. 7.

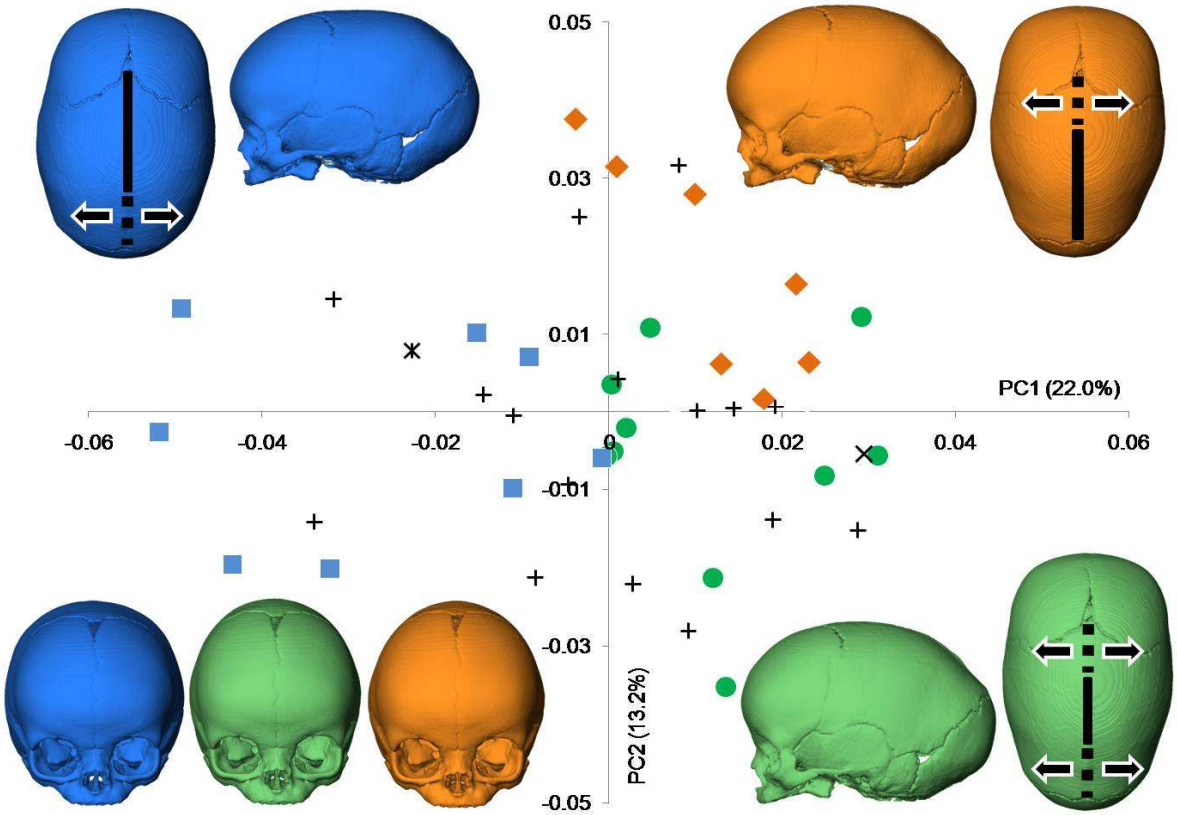

Supplementary data 3

Superimposed Procrustes average shape (PAS) of the skulls according to their sagittal suture closure pattern. PAS of the skulls with the closure pattern FFC is represented in blue. PAS of the skulls with the closure pattern CFC is represented in green. PAS of the skulls with the closure pattern CFF is represented in orange. Note that a single skull with the closure pattern FFF has been warped to create the PASs skulls represented here. Consequently, the sagittal suture closure pattern of the PASs' representations do not correspond to the reality. The visible parts of the PAS correspond to the ones that are the closest to the eye of the observer. For example the orange PAS presents a wider and more anteriorly projected frontal than the blue PAS.

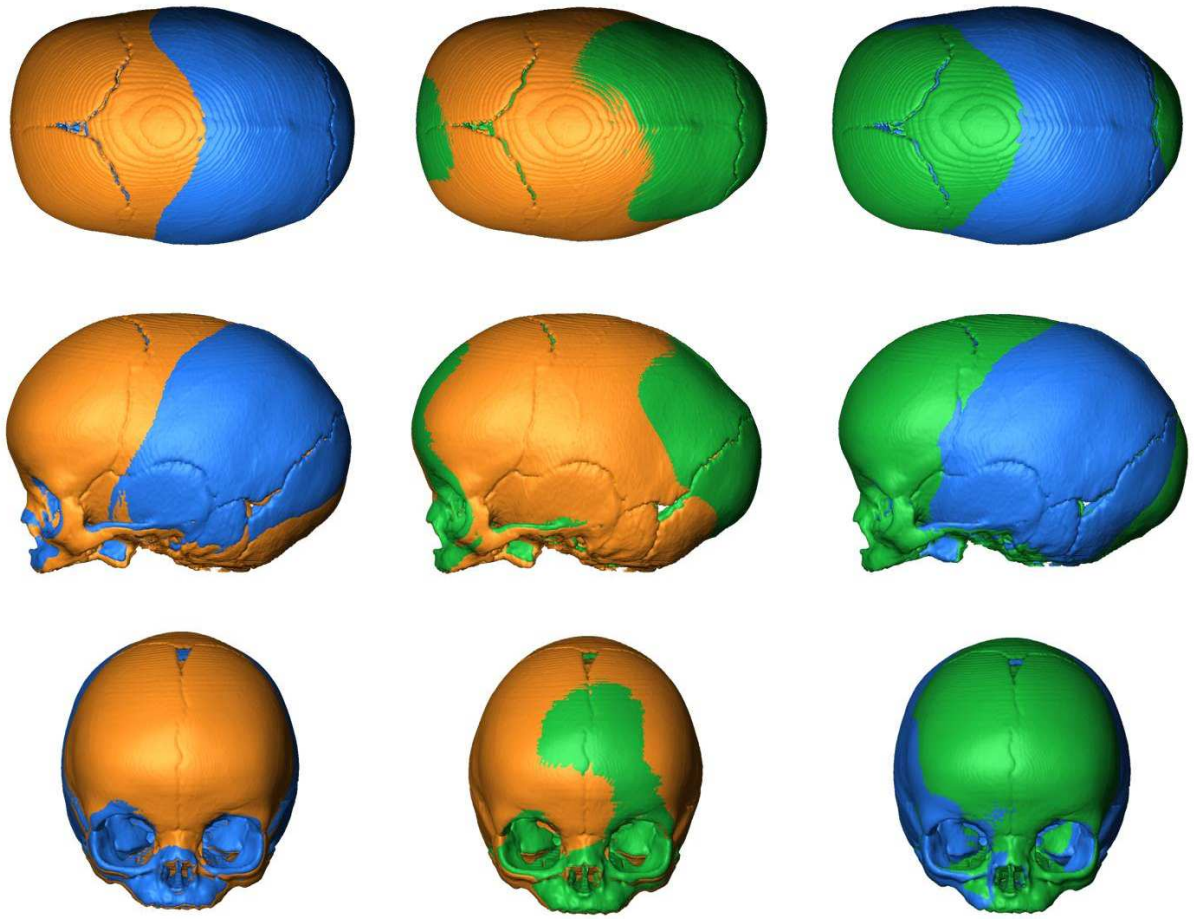

Table 1 Sample sex and age description. The closure pattern of the sagittal suture is indicated (C: closed, F: fused) as well as deciduous maxillary first molar (m^1) dental stages. Observations are grouped by sagittal suture closure pattern. Relative proportions and mean age for each group are presented.

Suture closure pattern (mean age in months)	Age (months)	AgeGroup (months)	Sex	m^1	Percentage
CCC	6.0	6-9	M	C	2.3
FCC	0.9	0-3	M	B	2.3
CFC (3.0)	1.1	0-3	M	C	23.3
	2.0	0-3	M		
	2.2	0-3	M	C	
	2.5	0-3	F	B	
	2.6	0-3	M	C	
	3.1	3-6	M	B	
	3.2	3-6	M	B	
	3.6	3-6	M	B	
	4.7	3-6	M	C	
	5.4	3-6	M	B	
CFF (4.9)	1.8	0-3	M	B	16.3
	3.3	3-6	F	C	
	4.1	3-6	M	B	
	4.7	3-6	M	C	
	5.2	3-6	M	D	
	7.2	6-9	M	C	
	8.0	6-9	M		
FFC (4.6)	2.3	0-3	M	B	18.6
	2.3	0-3	M		
	2.5	0-3	M	B	
	3.6	3-6	M	C	
	4.6	3-6	F	B	
	5.2	3-6	M	C	
	7.2	6-9	M	C	
	8.7	6-9	F	C	
FFF (5.8)	3.3	3-6	M	B	37.2
	3.4	3-6	M	C	
	3.5	3-6	M	C	
	3.5	3-6	F	B	
	4.0	3-6	M	B	
	4.8	3-6	M	C	
	5.0	3-6	M	C	
	5.7	3-6	F	C	
	6.1	6-9	F	D	

6.3	6-9	M	C
6.6	6-9	M	D
7.0	6-9	M	D
7.4	6-9	M	D
8.3	6-9	M	C
8.5	6-9	M	C
9.0	6-9	F	C

Table 2 Anatomical landmarks used in the study. Description is provided for points that have multiple or ambiguous definitions. Points without description are classic landmarks whose definitions can be found in Howells (1973) or at http://www.getahead.psu.edu/LandmarkNewVersion/Humanskull_Applet.html

Anatomical Landmark	Description
Anterior clinoid process L, R	
Anterior nasal spine	
Asterion L, R	
Basion	
Bregma	
Dorsum sellae	
Fissura orbitalis inferior L, R	*Sutura* sphenozygomatic (facial view)
Fissura orbitalis superior L, R	*Sutura* sphenofrontalis (facial view)
Foramen infra orbitary L, R	
Foramen ovale L, R	Most anterior part
Hormion	Most posterior midline point on vomer
Internal auditory meatus L, R	Most postero-lateral point
Lambda	
Nasale	
Nasion	
Opisthion	
Posterior nasal spine	Most posterior midline point on palatin
Pterigoid hamulus L, R	Most postero-inferior point
Sellae fossa hypophysialis	
Sutura fronto zygomatic L, R	On the orbit
Sutura maxillo zygomatic inferior L, R	Actually measured on the nearby processus
Sutura occipital temporal L, R	Around the foramen jugulare (ectocranial view)

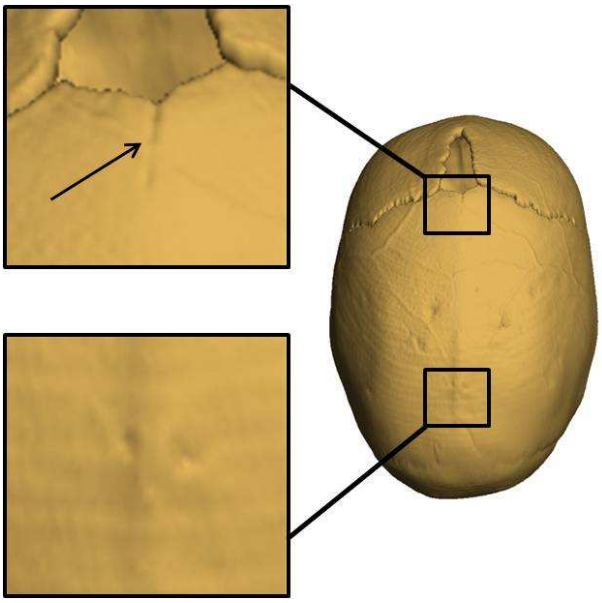

Fig. 1 Superior view of a sagittal suture (anterior fontanelle at top) illustrating sagittal suture closure pattern. Anterior section of sagittal suture “closed” (C), central and posterior section “fused” (F). Consequently, the closure pattern of the sagittal suture is CFF. The black arrow indicates appearance of suture sections we coded as “closed”.

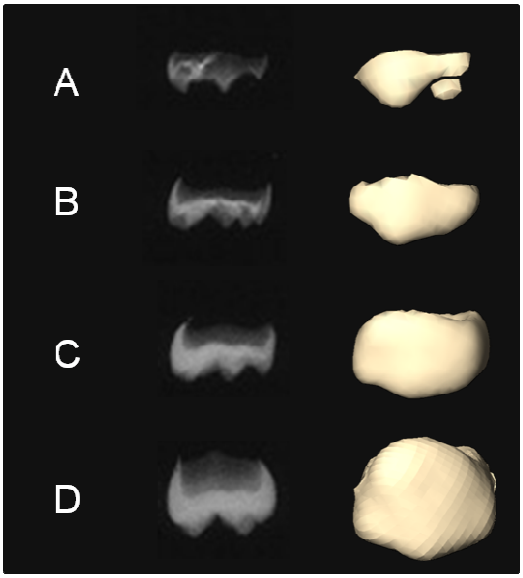

Fig. 2 Radiograph and 3D CT surface reconstruction of crown stages showing deciduous first molar. Stage A: beginning of mineralization at cusp tips, Stage B: coalescence of cusp tips to form a regularly outlined occlusal surface, Stage C: occlusal surface is complete. Approximal edges of forming crown has reached future contact areas, Stage D: crown (enamel) is complete with full-thickness occlusal dentine present, and roof of the pulp chamber is mature. Beginning of root formation is seen (modified after Liversidge & Molleson, 2004).

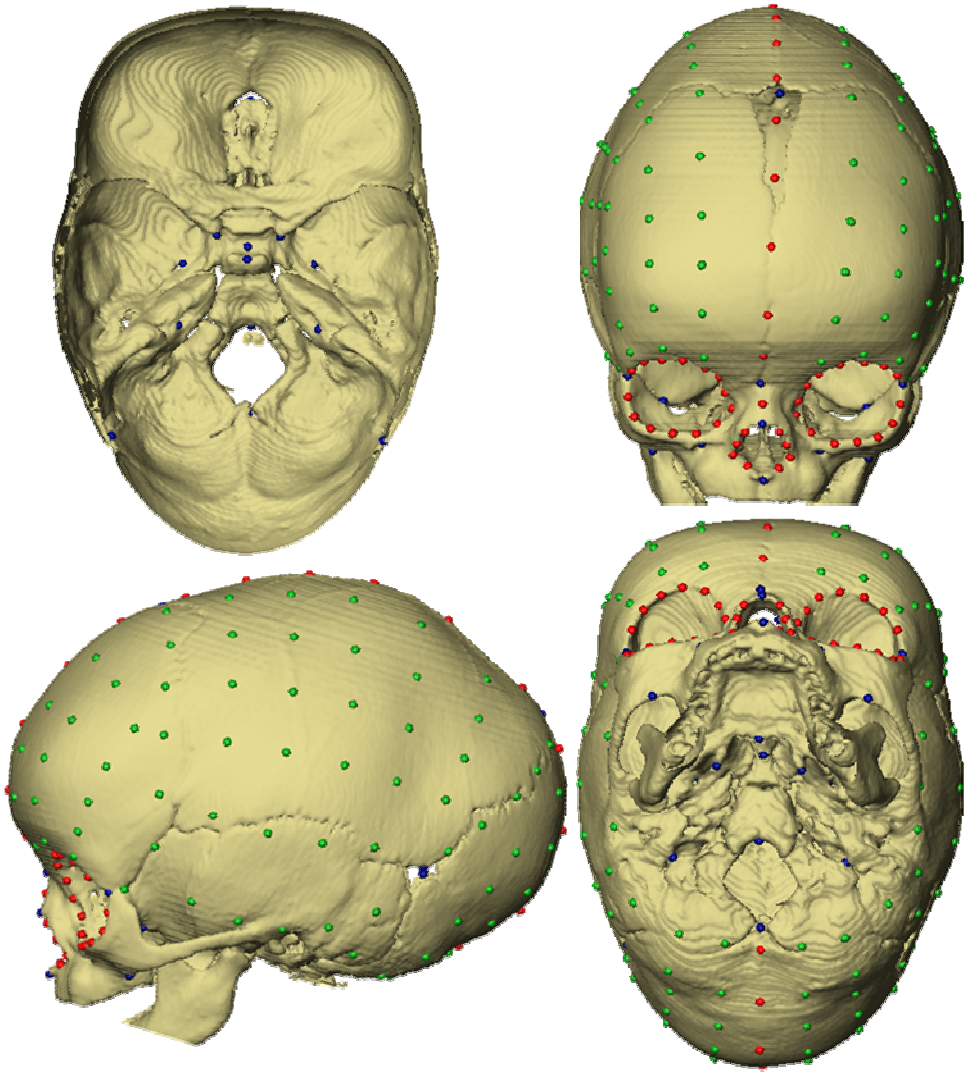

Fig. 3 Illustration of the 222 points measured on 3D reconstruction of computed tomography scans of each individual in our sample. Anatomical landmarks (Table 2) are shown in blue, curve semilandmarks are shown in red, and surface semilandmarks are shown in green. Top left: endocranial surface of the cranial base, top right: anterior view, bottom left: lateral view, bottom right: inferior view.

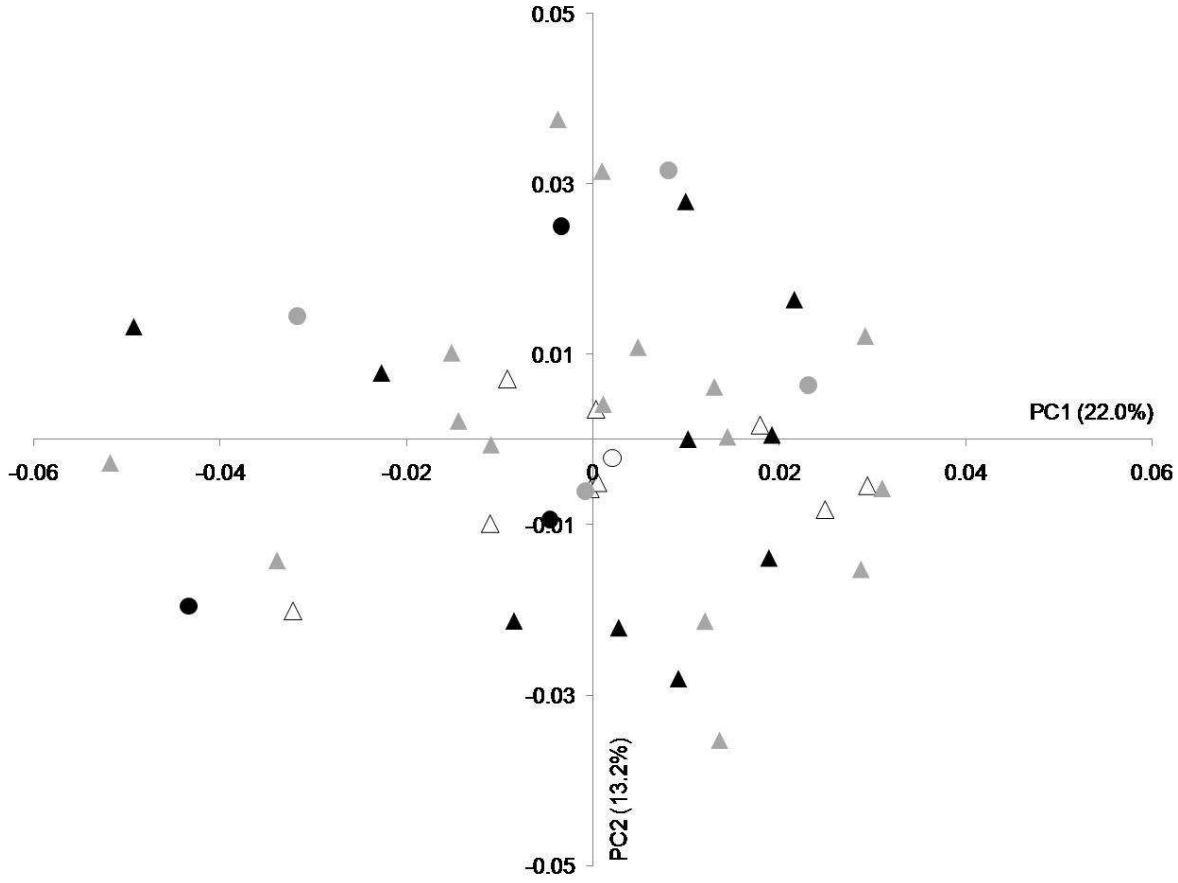

Fig. 4 Placement of the individuals on PC1 and PC2 in the shape space (principal components analysis of the Procrustes shape coordinates using all landmarks and semilandmarks of the 43 infants with sagittal NSC). Male infants are denoted by triangles while circles denote female infants. Ages of individuals are indicated by colour: white = 0-3 months, grey = 3-6 months, black = 6-9 months.

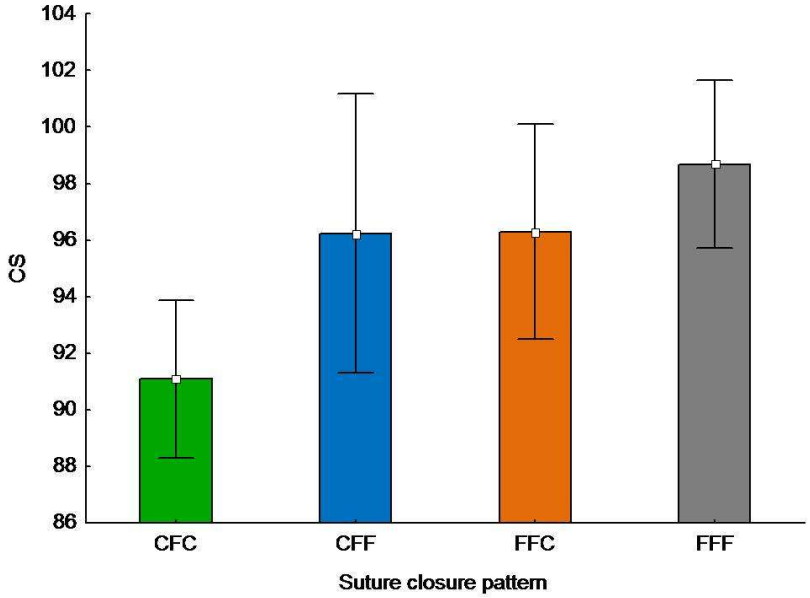

Fig. 5 Mean and 0.95 confidence interval plot of centroid size (CS) grouped by sagittal suture closure pattern (C: closed, F: fused).

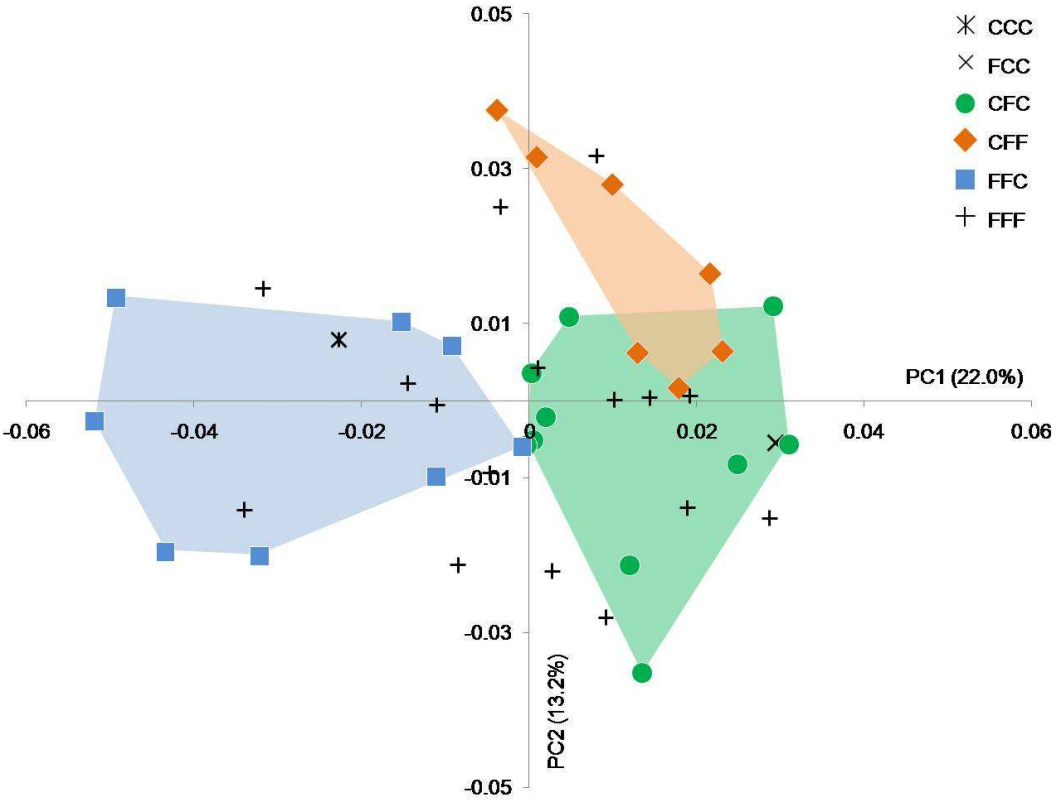

Fig. 6 Placement of the individuals on PC1 and PC2 in the shape space defined by the principal components analysis of the Procrustes shape coordinates using all landmarks and semilandmarks of the 43 infants with sagittal NSC. Individuals are coded for suture closure pattern (closed: C, fused: F). Convex hulls (transparent) are drawn for the CFC, CFF and FFC groups.

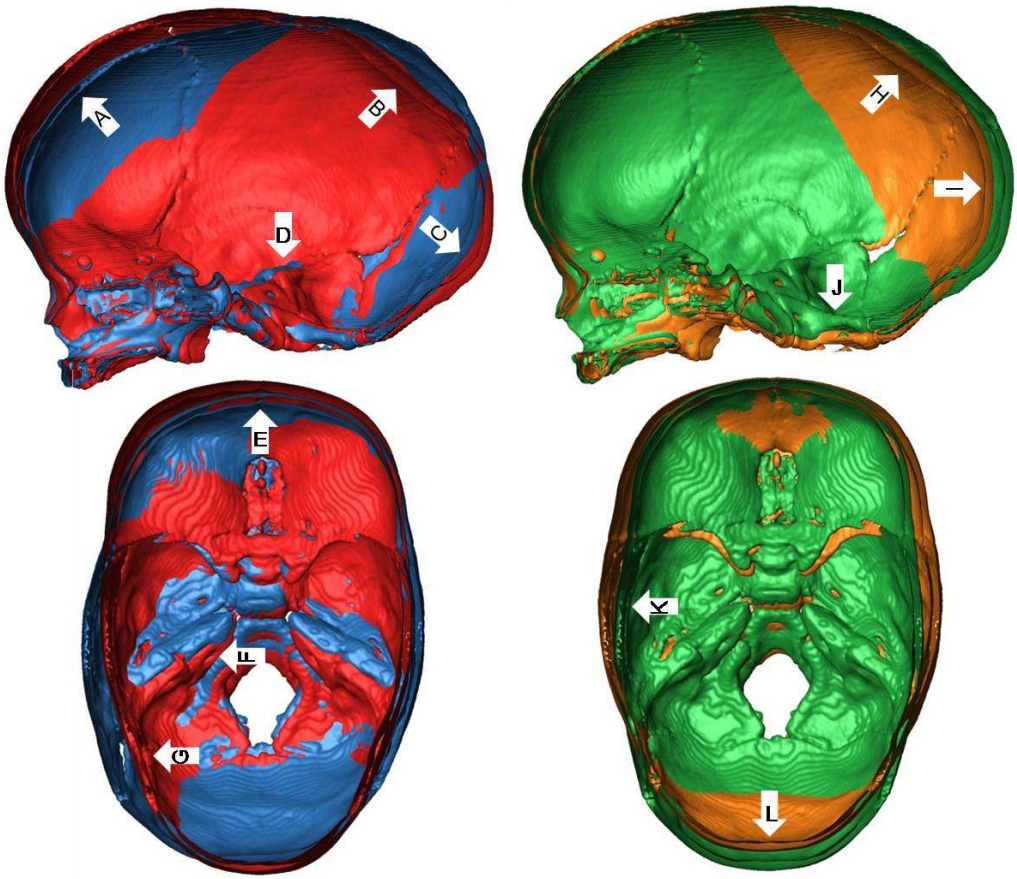

Fig. 7 Superimposed warped skulls according to PC1 (left) and PC2 (right). Lateral views of endocranial surface viewed through a mid-sagittal section (top) and superior view of endocranial surface of axial sections (bottom). The blue warped skull corresponds to -0.05PC1 and the red warped skull corresponds to +0.04PC1. The green warped skull corresponds to -0.04PC2 and the orange warped skull corresponds to +0.04PC2. The colours of the warped skulls (i.e. blue, orange and green) correspond to the colours used in fig. 6. Arrows show the main shape differences (see text for more details).

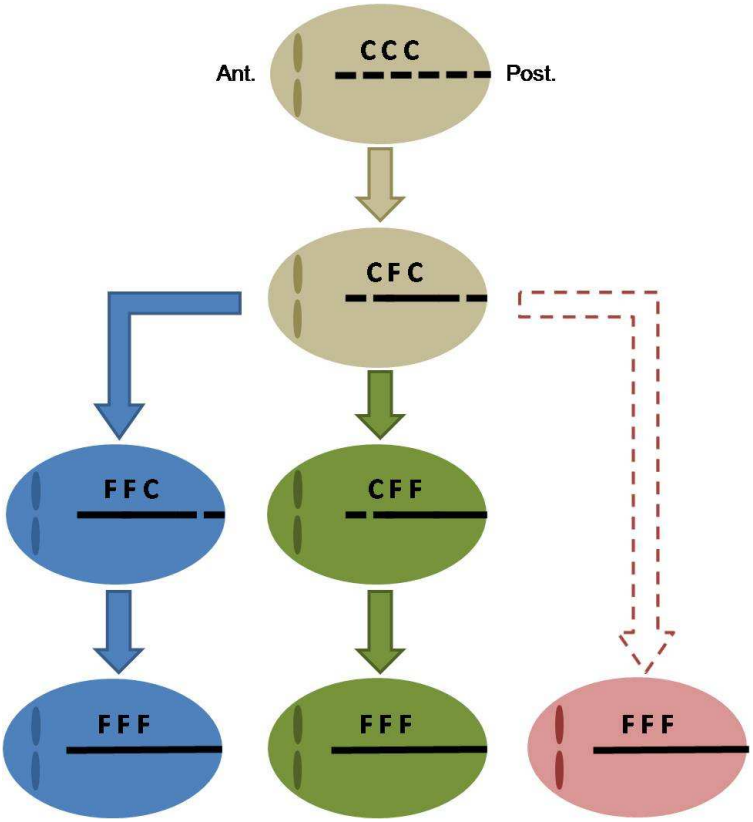

Fig. 8 Illustrations of three potential closure pattern sequences of the sagittal suture in sagittal NSC cases as documented in our study. The sagittal suture is divided into three distinct sections: anterior, median, and posterior. Each section is coded as closed (C) or fused (F).